Nanoscale

ROYAL SOCIETY OF CHEMISTRY

PAPER

View Article Online
View Journal | View Issue

Cite this: *Nanoscale*, 2020, **12**, 7263

Perovskite hetero-anionic-sublattice interfaces for optoelectronics and nonconventional electronics†

Dali Cheng,[a] Deying Kong,[b] Xing Sheng,[a,c] Lan Yin[b] and Huanglong Li *[d]

The perovskite structure provides a versatile framework for functional materials and their high-quality heteroepitaxial interfaces. Perovskite halides (PH) have attracted intense interest for their application in optoelectronics. Oxides are another major class of perovskites that are widely used in fuel cells, nonconventional electronics and electrochemistry. Interfacing different perovskite oxides (POs) has led to a multitude of fascinating discoveries. By introducing anionic degree of freedom, we expect that perovskite hetero-anionic-sublattice interfaces can provide a new platform for emergent phenomena that may or may not have homo-oxygen-sublattice interface analogues. In this work, we investigate the interfaces between the all-inorganic PH $CsPbBr_3$, the emerging double perovskite halide (dPH) Cs_2TiBr_6 and various common POs. Based on the band alignment properties, these POs are considered to be suitable carrier transport materials (CTMs) for $CsPbBr_3$ and Cs_2TiBr_6 in either light-harvesting or light-emitting devices. In addition, these perovskite hetero-anionic-sublattice interfaces are found to be defect- and dangling bond-free due to compatible crystal lattices, making POs potentially outperform conventional binary transition-metal–oxide and organic CTMs. Besides optoelectronics, the potential of perovskite hetero-anionic-sublattice interfaces for nonconventional electronics is also explored. As examples, two-dimensionally confined electron–hole systems are predicted at the asymmetric interfaces in both Cs_2TiBr_6:$LaAlO_3$ and $CsPbBr_3$:$LaAlO_3$ superlattice structures. This finding, along with the optically active properties of PHs, may spark novel applications of light–electron interaction in perovskite systems. This work presents new opportunities for perovskite heteroepitaxial interfaces.

Received 30th August 2019,
Accepted 26th February 2020

DOI: 10.1039/c9nr07475a

rsc.li/nanoscale

Introduction

Perovskite materials have been extensively studied for a wealth of applications. The common chemical formula of perovskites is ABX_3, where A and B are two cations of different sizes and X is an anion. The freedom of composition gives rise to an exceptional diversity of material properties and thus a wide range of applications. In the past decade, perovskite optoelectronics based on halides has continued to make sweeping strides due to a combination of high-quality light–electric power conversion and the ease of fabrication.[1,2] Despite the rapid surge in the record power conversion efficiency of organic–inorganic hybrid perovskites, several major problems remain to be resolved, including particularly the long-term chemical instability due to the intrinsic structural disorder in the strongly polar organic molecular and structurally dynamic inorganic frameworks, and the inclusion of toxic lead (Pb).[3] The substitution of organic components with inorganic cesium (Cs) has been considered to be a possible approach to improve the environmental tolerance of the perovskite films.[4] $CsPbX_3$ (X: Cl, Br, and I) have superior thermal stabilities compared to their organic–inorganic hybrid counterparts and their photophysical properties are also promising. To eliminate Pb, it has been shown that tin (Sn), germanium (Ge), bismuth (Bi), antimony (Sb), indium (In), and silver (Ag) are viable replacements.[5,6] Titanium (Ti) is a recent entry to the list.[7–9] The double perovskite halide (dPH) Cs_2TiX_6 has recently been reported with integrated advantages of cost-effectiveness, nontoxicity, stability and bandgap tunability. dPH Cs_2TiX_6 is a derivative of the conventional perovskite halides (PH), in which every other Ti^{4+} cation is missing. The dPH solid-state framework results in isolated $[TiX_6]^{2-}$ octahedra but the close-packed anionic sublattice familiar to PHs is still retained.

Interfacing different functional materials and engineering their interface properties is the workhorse of modern device technologies in different fields, including solar cells and light-

[a]*Department of Electronic Engineering, Tsinghua University, Beijing 100084, China*
[b]*School of Materials Science and Engineering, Tsinghua University, Beijing 100084, China*
[c]*Beijing National Research Center for Information Science and Technology, Tsinghua University, Beijing 100084, China*
[d]*Department of Precision Instrument, Tsinghua University, Beijing 100084, China. E-mail: li_huanglong@mail.tsinghua.edu.cn*

†Electronic supplementary information (ESI) available. See DOI: 10.1039/c9nr07475a

emitting (LE) diodes.[10–13] In a perovskite optoelectronic device, the perovskite light absorber (emitter) material (or active material, AM) is typically sandwiched between a hole transport material (HTM) and an electron transport material (ETM) for efficient carrier extraction (injection). Binary transition-metal oxides (TMOs) and organics are most widely employed in current devices as ETMs and HTMs, respectively. However, the non-perovskite structures of these binary TMOs result in perovskite:ETM interfaces that are prone to defects and dangling bonds or wrong bonds, while the organic HTMs are sensitive to moisture and oxygen.[14] Outweighing the benefits of perovskites, these have led to performance degradation in devices.

In addition to PHs, oxides are another major, perhaps the most common class of perovskites. Perovskite oxides (POs) exhibit a large variety of physical and chemical properties and are widely used in fuel cells, electronics and catalysis. The similar crystal lattices provide the advantage of interfacing different POs in an atomically precise epitaxial way. In fact, heteroepitaxial PO interfaces are the birthplace of numerous fascinating discoveries in fundamental science, such as high-mobility two-dimensional electron/hole gas (2DEG/2DHG) and two-dimensional superconductivity at interfaces between two insulators, artificial multiferroics and improper ferroelectricity.[15–18]

Despite being the main members of the perovskite family, halides and oxides have rarely met each other in the previous research. There are limited works on using POs as ETMs in PH-based photovoltaic (PV) cells.[19–21] In fact, POs could provide more possibilities to change the bandgap, work function and electrical conductivity than the binary TMOs. In addition, the all-perovskite heterointerfaces could be of better epitaxial quality to boost the performance of halide-based optoelectronic devices.[22,23] Moreover, the difference from both anionic and cationic sublattices across the interface potentially provides richer interface chemistry, which may give rise to plenty of new phenomena that may or may not have homo-oxygen-sublattice interface analogues.

There are also several major issues to be addressed before POs can meet the requirements of the CTMs in practical applications: the synthesis of ternary oxides and the control of their composition. In addition, to apply ternary oxides as efficient CTMs in flexible, low-cost, and large-scale devices, it requires that the ternary oxides be deposited by solution process techniques at low temperature.[23]

As preliminary research, we investigated the interfaces between the all-inorganic PH $CsPbBr_3$, the emerging dPH Cs_2TiBr_6 and various common POs in this work. The suitability of these POs for $CsPbBr_3$- and Cs_2TiBr_6-based optoelectronics is evaluated based on the interfacial properties. Besides optoelectronics, the potential of perovskite hetero-anionic-sublattice interfaces for nonconventional electronics is also explored in both Cs_2TiBr_6:$LaAlO_3$ and $CsPbBr_3$:$LaAlO_3$ example superlattice structures. Thanks to the richness of the perovskite library, perovskite hetero-anionic-sublattice interfaces may give birth to various emergent phenomena and novel developing applications, such as optically tunable perovskite electronics.

Results and discussion

Bulk properties of PH, dPH and POs

The atomic structures and electronic structures of $CsPbBr_3$ and Cs_2TiBr_6 are illustrated in Fig. 1. In Cs_2TiBr_6, whose chemical composition conforms to the A_2BX_6 formula, A-sites are fully occupied by Cs^+ cations while only half of the B-sites are occupied by Ti^{4+} cations, resulting in periodic structural vacancies on B-sites. The calculated band structure shows that Cs_2TiBr_6 has a band gap of around 1.61 eV. This band gap value is underestimated due to the limitations of the GGA functional.[7–9] The band gap is found to be quasi-direct with its valence band maximum (VBM) at Γ point and conduction band minimum (CBM) at X point which has slightly lower energy (65 meV) than Γ point. The projected densities of states (PDOSs) show that the VBM and CBM are mainly of the p and d state character of Br and Ti, respectively. The s states of Cs lie high in the CB.

On the other hand, $CsPbBr_3$ has the typical perovskite structure and the calculated band gap is around 1.80 eV, which is smaller than the experimental value.[24] The band gap is direct, with both the VBM and CBM at R point. The VBM is mainly from the Br p and Pb s states, and the CBM is from the Pb p state.

In this work, we mainly focus on three typical classes of POs, namely, Ti-based $ATiO_3$ (A: Ca, Sr, and Ba), Zr-based $AZrO_3$ (A: Ca, Sr, and Ba) and $LaAlO_3$. The electronic structures of these seven POs to be interfaced with PH $CsPbBr_3$ and dPH Cs_2TiBr_6 are shown in Fig. S1.† $ATiO_3$ have band gaps of approximately 2.0 eV, while $AZrO_3$ and $LaAlO_3$ have larger band gaps of about 3.5 eV. These band gap values are underestimated compared with the experimental values.[25–27] For $ATiO_3$ and $AZrO_3$, similar to Cs_2TiBr_6, the VBM is mainly of the p state character of anionic O, and the CBM is mainly contributed by B-site cations. The s states of A-site cations lie relatively higher in the CB. In contrast, the CBM of $LaAlO_3$ is mainly of the d state character of A-site La while the s states of B-site Al lie high in the CB.

PH:PO and dPH:PO interfaces for optoelectronics

We first investigated the band alignment properties of various Cs_2TiBr_6:$A^{2+}B^{4+}O_3$ interfaces and evaluated the suitability of these POs as carrier transport materials (CTM) for Cs_2TiBr_6-based optoelectronic devices. According to the calculated lattice constants of the selected POs (see Table S1†), Cs_2TiBr_6:PO interfaces with good lattice matching are constructed by a 45-degree rotation of the PO unit cell lattices around their ⟨001⟩ axes relative to the Cs_2TiBr_6 lattices. Two periods of the redefined PO lattices parallel to the interfaces (perpendicular to the ⟨001⟩ axis) are then subjected to strains to match the unit cell lattices of Cs_2TiBr_6. In geometry optimization, the lattices parallel to the interfaces are fixed and the lattices perpendicular to the interfaces are optimized. In this way, the effects of strain parallel to the interfaces are partly compensated. To

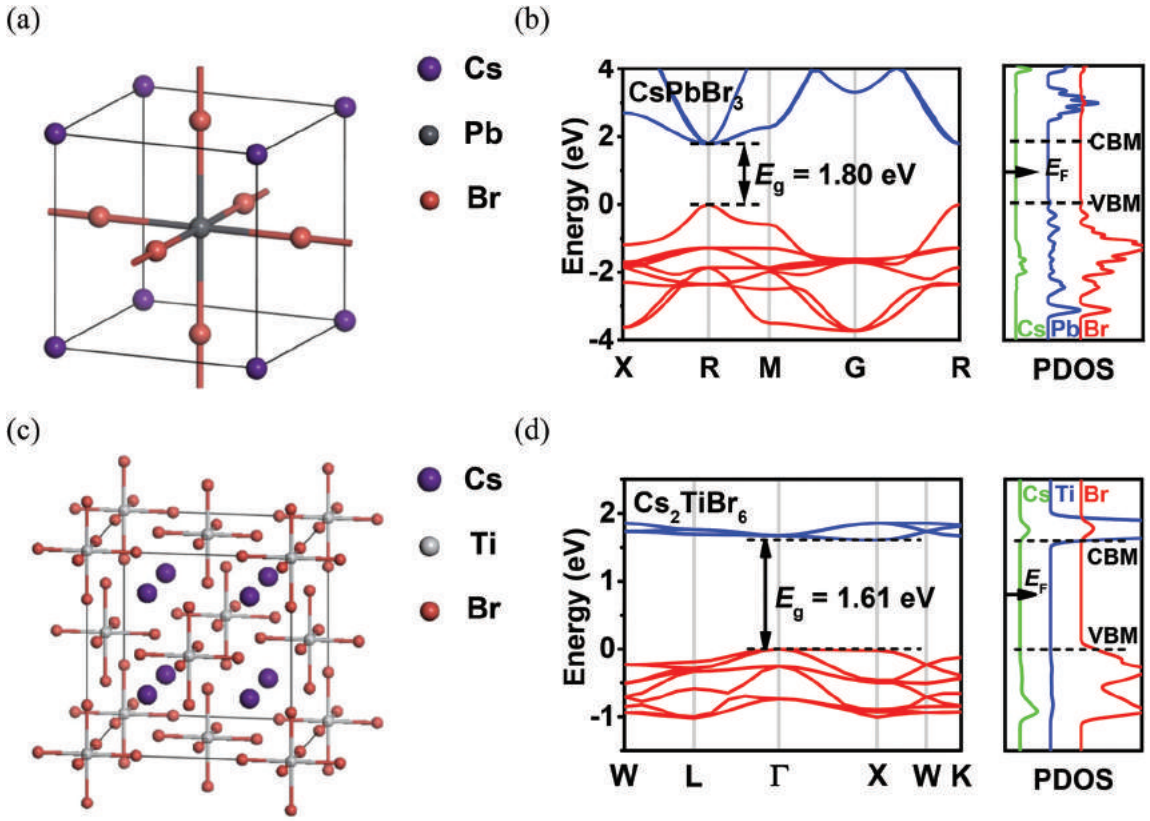

Fig. 1 (a) Atomic structure of PH $CsPbBr_3$. (b) Band structure and PDOSs of $CsPbBr_3$. (c) Atomic structure of dPH Cs_2TiBr_6. (d) Band structure and PDOSs of Cs_2TiBr_6.

confirm, we use the unit cells of $SrTiO_3$ as examples which are subjected to biaxial strains of the same strengths as those at the Cs_2TiBr_6:$SrTiO_3$ and $CsPbBr_3$:$SrTiO_3$ interface models, respectively. Cell optimizations are then performed with the pre-strained lattices fixed. The resulting PDOSs are comparable with that of the unstrained $SrTiO_3$ (see Fig. S2†). The ABAB... sequential layer order of the perovskite can be preserved at the interface in two different ways, namely, interfacing the A-site layer of Cs_2TiBr_6 with the B-site layer of PO (type-a), or the B-site layer of Cs_2TiBr_6 with the A-site layer of PO (type-b), as shown in Fig. S3.† The desired AM:ETM and AM:HTM interfaces should be free of electrically active defects. The compatible crystal lattices of Cs_2TiBr_6 and the POs under investigation are beneficial for minimization of the amount of wrong bonds as possible detrimental defects at the Cs_2TiBr_6:PO interfaces. To ensure insulation, the stoichiometries of the interfaces should satisfy the valence-counting rule. To achieve this, for the type-a interface, two Cs atoms and one Br atom from the terminated A-site layer of dPH are removed and one O atom from the terminated B-site layer of PO is replaced by one Br atom; while for the type-b interface, the valence-counting rule is naturally satisfied.

On the other hand, the $CsPbBr_3$:$A^{2+}B^{4+}O_3$ interfaces are built by matching one period of the 45-degree rotated PO unit cell lattices with the unit cell lattices of $CsPbBr_3$. To satisfy the valence-counting rule, one Cs atom from the terminated A-site layer of PH is removed and one O atom from the terminated B-site layer of PO is replaced by one Br atom for the type-a interface; for the type-b interface, the valence-counting rule is naturally satisfied.

The stabilities of these interfaces are evaluated by using the interface formation energy according to:

$$E_{\text{formation}} = \tfrac{1}{2}\{E^{\text{tot}}[\text{interface}] - n_{\text{halide}}E^{\text{tot}}[\text{halide}] - n_{\text{oxide}}E^{\text{tot}}[\text{oxide}] - \sum n_i\mu_i\} \quad (1)$$

where E^{tot}[interface] is the calculated total energy of the interface system, E^{tot}[halide] and E^{tot}[oxide] represent the total energies of the (d)PH and PO unit cells respectively, n_{halide} and n_{oxide} represent the numbers of the (d)PH and PO unit cells composing the interface system, and n_i is the number of of atoms of element i that is added (positive n_i) or removed (negative n_i), and μ_i denotes the chemical potential of atom i. The coefficient $\frac{1}{2}$ accounts for two identical interfaces in each model. The chemical potentials of the atomic constituents are allowed to vary over a restricted range determined by equilibrium thermodynamics, bound by the conditions that (i) will not cause the precipitation of solid elemental A (A: Ca, Sr, Ba, Cs, and La), solid elemental B (B: Ti, Zr, Pb, and Al), and molecular X (X: O and Br), *i.e.*,

$$\mu_A < \mu_A^{\text{crystal}}, \mu_B < \mu_B^{\text{crystal}}, \mu_X < \mu_{X2}^{\text{molecule}} \quad (2)$$

(ii) maintain the stable ABX_3 (or A_2BX_6), *i.e.*,

$$\mu_A + \mu_B + 3\mu_X = \mu_{ABX_3}^{crystal} \text{ or } 2\mu_A + \mu_B + 6\mu_X = \mu_{A_2BX_6}^{crystal} \quad (3)$$

(iii) will not cause the formation of solid binaries AO and BO_2 (or CsBr and $TiBr_4$/$PbBr_2$ for Cs_2TiBr_6/$CsPbBr_3$, or La_2O_3 and Al_2O_3 for $LaAlO_3$), *i.e.*,

$$\begin{aligned}&\mu_A + \mu_O < \mu_{AO}^{crystal}, \mu_B + 2\mu_O < \mu_{BO_2}^{crystal},\\ &\text{or } \mu_{Cs} + \mu_{Br} < \mu_{CsBr}^{crystal}, \mu_{Ti} + 4\mu_{Br} < \mu_{TiBr4}^{molecule}/\mu_{Pb} + 2\mu_{Br} < \mu_{PbBr_2}^{crystal},\\ &\text{or } 2\mu_{La} + 3\mu_O < \mu_{La_2O_3}^{crystal}, 2\mu_{Al} + 3\mu_O < \mu_{Al_2O_3}^{crystal}\end{aligned} \quad (4)$$

The calculated ranges of atomic chemical potentials for Cs_2TiBr_6, $CsPbBr_3$, and various POs are shown on their corresponding two-dimensional "μ_A *vs.* μ_X" planes in Fig. S4 (a–h).† Labelled points on the boundaries represent Br-rich (point A) and Br-poor (point B) extreme conditions for (d)PH, and O-rich (point C) and O-poor (point D) extreme conditions for POs. It should be noted that the determination of atomic chemical potentials in Cs_2TiBr_6:$ATiO_3$ interface systems is slightly different because Ti is the common element of the two interface components. The allowed ranges of chemical potentials are determined by:

$$\begin{aligned}&\mu_{Cs} < \mu_{Cs}^{crystal}, \mu_{Ti} < \mu_{Ti}^{crystal}, \mu_{Br} < \mu_{Br_2}^{molecule}, \mu_A < \mu_A^{crystal},\\ &\mu_O < \mu_{O_2}^{molecule}, \mu_{Cs} + \mu_{Br} < \mu_{CsBr}^{crystal}, \mu_{Ti} + 4\mu_{Br} < \mu_{TiBr_4}^{molecule},\\ &\mu_A + \mu_O < \mu_{AO}^{crystal}, \mu_{Ti} + 2\mu_O < \mu_{TiO_2}^{crystal},\\ &2\mu_{Cs} + \mu_{Ti} + 6\mu_{Br} = \mu_{Cs_2TiBr_6}^{crystal}, \mu_A + \mu_{Ti} + 3\mu_O = \mu_{ABO_3}^{crystal}\end{aligned} \quad (5)$$

The calculated ranges of atomic chemical potentials for Cs_2TiBr_6:$ATiO_3$ interfaces are shown on their corresponding three-dimensional "μ_O–μ_{Br}–μ_{Cs}" color contour plots in Fig. S4 (i–n).†

It is found that the type-b Cs_2TiBr_6:$AZrO_3$, $CsPbBr_3$:$ATiO_3$ and $CsPbBr_3$:$AZrO_3$ interfaces are generally more stable than their type-a counterparts which are stable only under O-poor and Br-rich conditions, whereas the type-b Cs_2TiBr_6:$ATiO_3$ interfaces are always more stable than their type-a counterparts regardless of the atomic chemical potentials. The interface formation energy values for different systems under extreme conditions are listed in Tables S2–S4.†

The interface formation energies can alternatively be associated with the surface energies of the two components and the energy gain during the formation of new interfacial chemical bonds, *i.e.*,

$$E_{formation} = E_{surface}[\text{halide}] + E_{surface}[\text{oxide}] - E_{bonds} \quad (6)$$

where $E_{surface}$ is the energy of the isolated surface on either side of the interface and E_{bonds} is the energy gain during the formation of interfacial chemical bonds.

The surface energies of Cs_2TiBr_6, $CsPbBr_3$ and various perovskite oxides have been calculated according to:

$$\begin{aligned}E_{surface}[\text{halide}] &= 1/2\{E^{tot}[\text{halide surface}]\\ &\quad - n_{halide}E^{tot}[\text{halide}] - n_{Cs}m_{Cs} - n_{Br}m_{Br}\}\\ E_{surface}[\text{oxide}] &= 1/2\{E^{tot}[\text{oxide surface}]\\ &\quad - n_{oxide}E^{tot}[\text{oxide}] - n_Am_A - n_Om_O\}\end{aligned} \quad (7)$$

where E^{tot}[halide surface] and E^{tot}[oxide surface] are the total energies of (d)PH and PO surfaces, respectively.

To form type-a interfaces, the A-site layer terminated (d)PH surfaces are generally stable under Br-rich conditions and the B-site layer terminated PO surfaces are stable under O-poor conditions. The formation of new interfacial chemical bonds is exothermic. On the other hand, to form type-b interfaces, surface energies are not strongly influenced by the atomic chemical potentials of Cs_2TiBr_6:$AZrO_3$, $CsPbBr_3$:$ATiO_3$ and $CsPbBr_3$:$AZrO_3$ interfaces and O-rich conditions are slightly favorable for the formation of A-site layer terminated PO surfaces. For type-b Cs_2TiBr_6:$ATiO_3$ interfaces, however, the B-site layer terminated dPH surfaces are stable under the Br-rich conditions and the A-site layer terminated PO surfaces are stable under the O-poor conditions. The formation of new interfacial chemical bonds is also exothermic. The surface energy values and the energy gain during the formation of interfacial chemical bonds for different systems under extreme conditions are listed in Tables S5–S7.†

To ensure high power conversion efficiency, the ETM and HTM should have proper band offsets with the AM. In particular, for LE applications, there should be no or minimum barrier at the AM:ETM (AM:HTM) interface for electron (hole) carrier injection into the AM; in other words, high-lying (low-lying) CBM (VBM) of the ETM (HTM) is preferred. In the meantime, there should be sufficiently large hole (electron) barrier at the AM:ETM (AM:HTM) interface to minimize hole (electron) current leakage from the AM, that is, low-lying (high-lying) VBM (CBM) of the ETM (HTM) is preferred. For PV applications, in contrast, low-lying (high-lying) band edges of the ETM (HTM) are favorable to induce asymmetric transport of electrons and holes which in turn favors electron (hole) extraction over hole (electron) extraction.

We first consider the suitability of $ATiO_3$ as CTMs. Fig. 2(a–f) show the PDOSs of the Cs_2TiBr_6:$ATiO_3$ interfaces. It is found that, by forming type-a and type-b interfaces, $ATiO_3$ have staggered and straddling band line-up with respect to Cs_2TiBr_6, respectively. In particular, in type-b interfaces, the CBMs of $ATiO_3$ are slightly higher than those of Cs_2TiBr_6 while the VBMs are lower by about 0.5 eV, being favorable to the injection of electrons into Cs_2TiBr_6 and in the meantime the suppression of hole leakage from Cs_2TiBr_6. Therefore, by forming type-b interfaces, $ATiO_3$ are considered to be suitable ETMs for LE devices. In comparison with their type-b counterparts, downward shifts of the CBMs/VBMs of $ATiO_3$ occur in type-a interfaces, resulting in slightly lower CBMs than those of Cs_2TiBr_6 and even larger VBOs. These are preferred for elec-

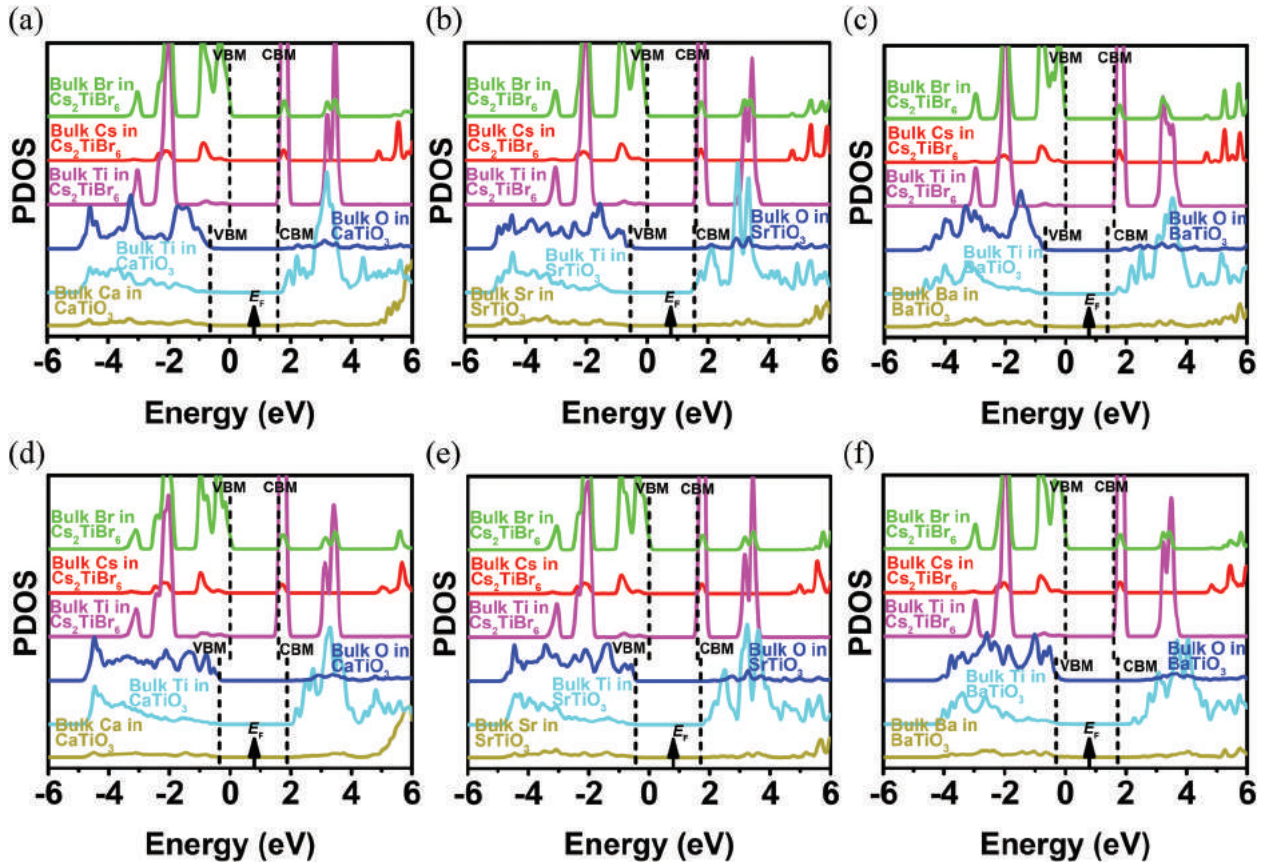

Fig. 2 PDOSs of (a) type-a and (d) type-b Cs_2TiBr_6:$CaTiO_3$ interfaces, (b) type-a and (e) type-b Cs_2TiBr_6:$SrTiO_3$ interfaces, and (c) type-a and (f) type-b Cs_2TiBr_6:$BaTiO_3$ interfaces.

tron extraction from Cs_2TiBr_6 while blocking holes. Therefore, by forming type-a interfaces, $ATiO_3$ are suitable as ETMs for PV applications.

We point out that the calculations should be considered more as qualitative than quantitatively accurate predictions of the band alignment properties. For ionic Cs_2TiBr_6 and various ABO_3 considered in this work, the trend of the energy levels of the anion p-states can be qualitatively well predicted by the GGA functional and thus the interface valence band offsets can be described with reasonable accuracy due to cancellation of errors in both interface components.[28]

We then consider $AZrO_3$. Fig. 3(a–f) show the PDOSs of the Cs_2TiBr_6:$AZrO_3$ interfaces. It is seen that both type-a and type-b Cs_2TiBr_6:$CaZrO_3$ interfaces show straddling band alignment with VBOs of less than 0.5 eV. On the other hand, Cs_2TiBr_6:$SrZrO_3$ and Cs_2TiBr_6:$BaZrO_3$ interfaces show staggered band alignment with the VBMs of ABO_3 higher than that of Cs_2TiBr_6. The CB offsets of all $AZrO_3$ with respect to Cs_2TiBr_6 are larger than 1.5 eV. These larger offset values compared with those of the Cs_2TiBr_6:$ATiO_3$ interfaces mainly arise from the larger band gap values of $AZrO_3$. Based on the characteristics of band alignment, $CaZrO_3$ is considered to be a suitable HTM for Cs_2TiBr_6-based LE devices that it allows hole injection into Cs_2TiBr_6 while suppressing electron leakage. $SrZrO_3$ and $BaZrO_3$, on the other hand, are preferred as HTMs for hole extraction from Cs_2TiBr_6 in PV applications. We also notice that, in contrast to Cs_2TiBr_6:$ATiO_3$ systems in which the bands of $ATiO_3$ in type-a interfaces are lower than those in type-b interfaces, Cs_2TiBr_6:$AZrO_3$ systems have higher lying $AZrO_3$ bands in type-a interfaces than in type-b interfaces.

When $CsPbBr_3$ is used as the AM, it is found that these POs are considered to be suitable HTMs for LE devices or ETMs for PV devices. To be specific, type-b $CsPbBr_3$:$AZrO_3$ interfaces have straddling band alignment with the CBOs of around 1.0 eV which are larger than the corresponding VBOs (Fig. 4). Therefore, $AZrO_3$ are considered to be suitable HTMs for $CsPbBr_3$-based LE devices by forming type-b interfaces that they allow hole injection into Cs_2TiBr_6 while suppressing electron leakage. On the other hand, type-a $CsPbBr_3$:$AZrO_3$ (Fig. 4) and type-b $CsPbBr_3$:$ATiO_3$ (Fig. 5) interfaces have staggered band alignment with the CBMs of POs lower than that of $CsPbBr_3$, and type-a $CsPbBr_3$:$ATiO_3$ (Fig. 5) interfaces have broken band alignment with the CBMs of POs even lower than the VBMs of $CsPbBr_3$. These are preferred ETM properties for electron extraction from $CsPbBr_3$ in PV applications. POs that are suitable as ETMs for LE devices and HTMs for PV devices are useful complements for $CsPbBr_3$-based optoelectronics and require further explorations.

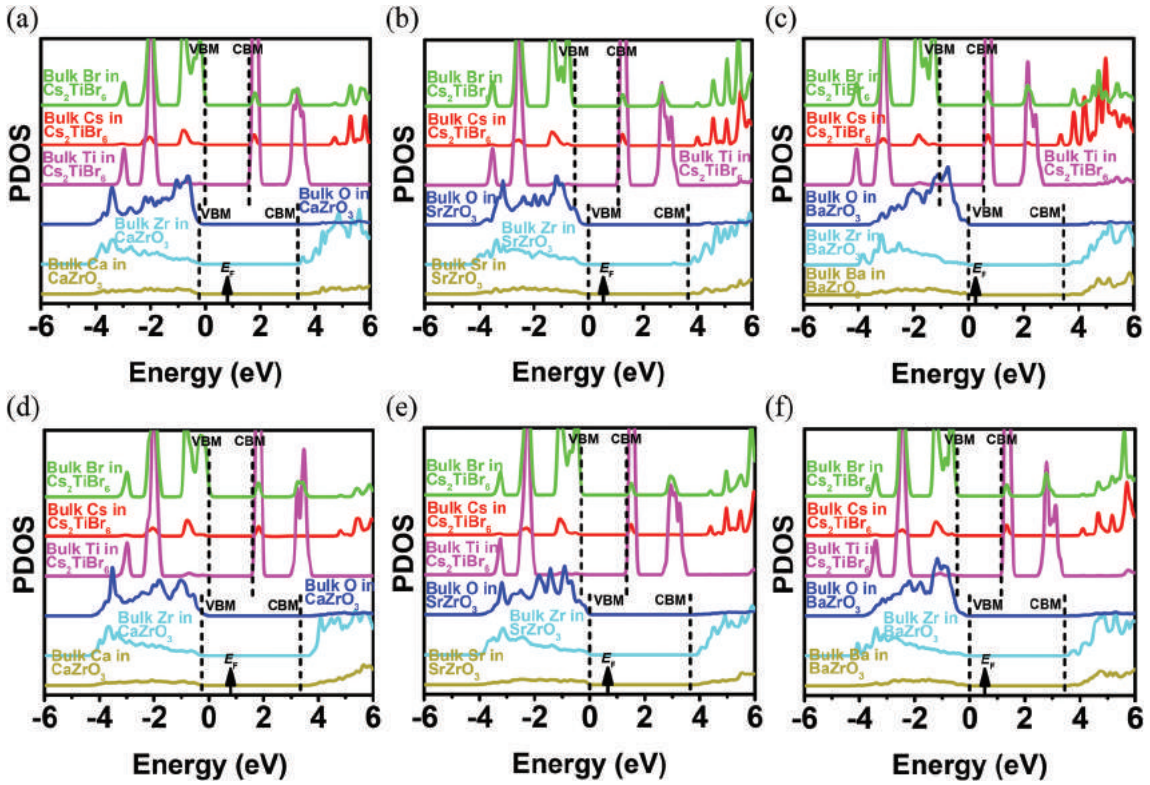

Fig. 3 PDOSs of (a) type-a and (d) type-b Cs_2TiBr_6:$CaZrO_3$ interfaces, (b) type-a and (e) type-b Cs_2TiBr_6:$SrZrO_3$ interfaces, and (c) type-a and (f) type-b Cs_2TiBr_6:$BaZrO_3$ interfaces.

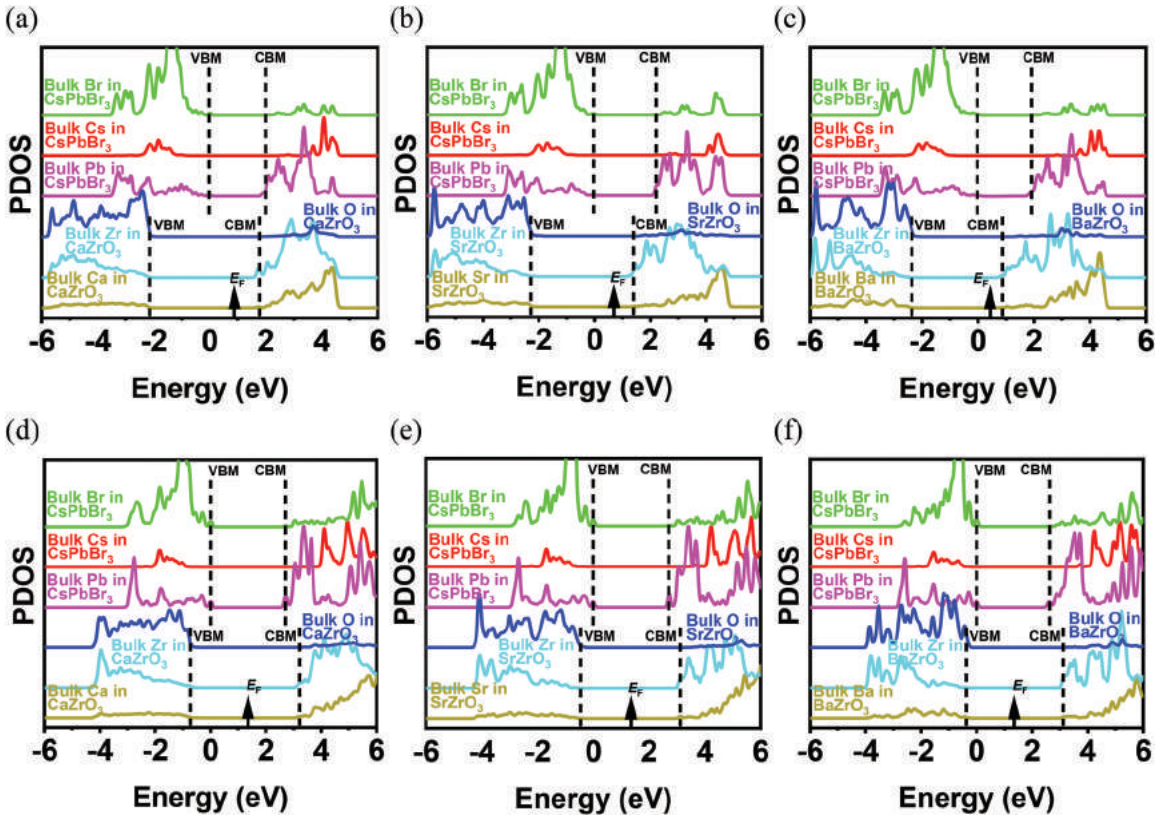

Fig. 4 PDOSs of (a) type-a and (d) type-b $CsPbBr_3$:$CaZrO_3$ interfaces, (b) type-a and (e) type-b $CsPbBr_3$:$SrZrO_3$ interfaces, and (c) type-a and (f) type-b $CsPbBr_3$:$BaZrO_3$ interfaces.

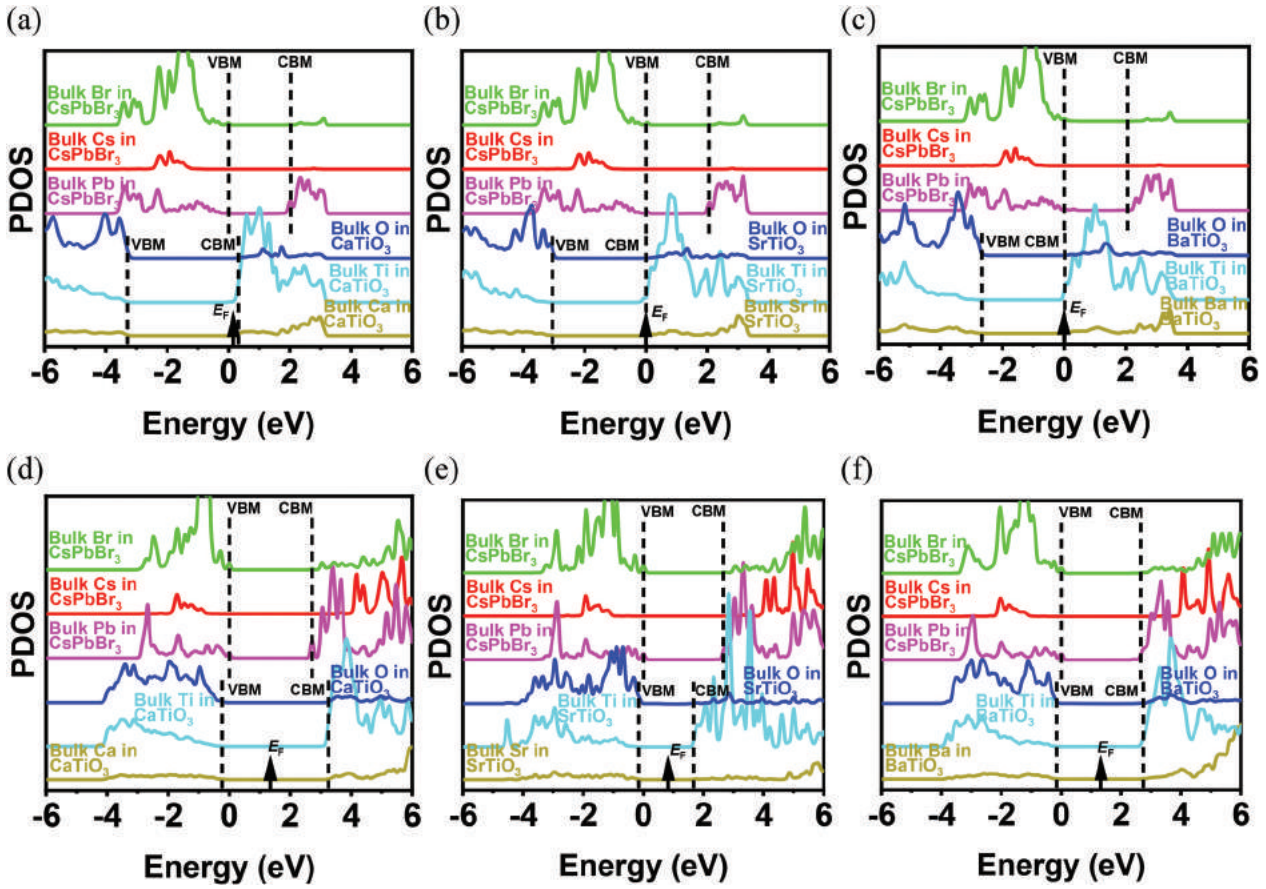

Fig. 5 PDOSs of (a) type-a and (d) type-b $CsPbBr_3$:$CaTiO_3$ interfaces, (b) type-a and (e) type-b $CsPbBr_3$:$SrTiO_3$ interfaces, and (c) type-a and (f) type-b $CsPbBr_3$:$BaTiO_3$ interfaces.

Before concluding this section, we would also like to identify some possible non-PO ETMs for the emerging Cs_2TiBr_6-based PV cells. ETMs for PV applications require simultaneous easy and suppressed electron and hole extraction from the AMs, that is, in terms of the interfacial electronic structures, staggered or broken band alignment with the VBMs of ETMs lower than those of the AMs. As aforementioned, TMOs such as TiO_2 are commonly used as ETMs in organic PH-based PV cells.[29–31] In contrast to the organic:TMO interfaces, Cs_2TiBr_6:TMO interfaces strongly interact with significant orbital hybridization that the band offsets cannot be predicted by simply aligning the vacuum levels.[32] The atomic and electronic structures of some typical TMO CTMs and their interfaces with Cs_2TiBr_6 are shown in Fig. S5 and S6,† respectively. TiO_2 is found to form broken band line-up with respect to Cs_2TiBr_6 with low-lying band edges, making it an effective ETM for PV applications. In addition, MoO_3, V_2O_5 and WO_3, which are usually HTMs in organic PV cells, have staggered band line-up (MoO_3 and V_2O_5) or broken band line-up (WO_3), with their CBMs lower than that of Cs_2TiBr_6, which is a desirable characteristic of ETMs for PV cells.[33,34] On the other hand, $SrCu_2O_2$ has staggered band line-up with high-lying CBM, making it useful as HTM for PV applications, similar to the case of cuprous oxides in organic PV. Fig. 6 summarizes the band alignment properties of the afore-studied Cs_2TiBr_6:ABO_3, Cs_2TiBr_6:TMO and $CsPbBr_3$:ABO_3 interfaces.

PH:PO and dPH:PO interfaces for nonconventional electronics

As mentioned earlier, extraordinary electron systems can be generated at the PO heteroepitaxial interfaces. The discovery of high-mobility or superconducting 2DEG between two POs has sparked extensive research in the emergent phenomena at the PO interfaces and development activities of novel oxide electronics.[35] The emergence of the 2DEG occurs when a charged atomic layer of one PO forms interface with a neutral layer of another PO, as a result of the so called "polar catastrophe".[36] Here, we investigate the possibility of forming 2DEG and 2DHG in Cs_2TiBr_6:$LaAlO_3$ and $CsPbBr_3$:$LaAlO_3$ superlattices.

Fig. 7(a) shows the atomic structure of a Cs_2TiBr_6:$LaAlO_3$ superlattice model with two asymmetric interfaces. The top interface is created between LaO^+ and neutral $TiBr_4$ layers, while the bottom interface is between AlO_2^- and neutral CsBr layers. The layer-by-layer PDOSs of this model are illustrated in Fig. 7(b). The obvious band tilting across Cs_2TiBr_6 and $LaAlO_3$ is an indication of the "polar catastrophe". In particular, the bands undergo upward tilting from the top interface to the bottom interface across $LaAlO_3$ but downward tilting across Cs_2TiBr_6 from the bottom interface to the top interface in the

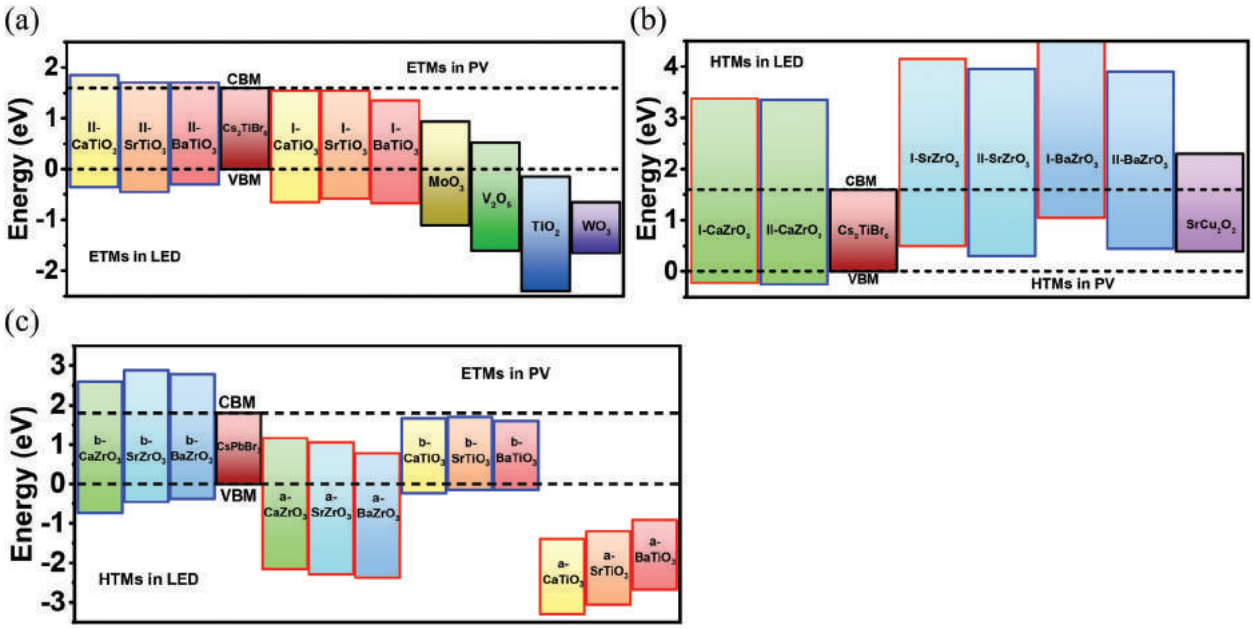

Fig. 6 Band alignment diagram of various (d)PH:PO interfaces and dPH:TMO interfaces. POs and TMOs are categorized into (a) ETMs and (b) HTMs for Cs_2TiBr_6-based LED (left) and PV (right) accordingly, and (c) HTMs for $CsPbBr_3$-based LED (left) and ETMs for $CsPbBr_3$-based PV (right). Band gaps of these investigated CTMs in type-a and type-b interfaces are indicated by red and blue borderlines, respectively. The VBM of (d)PH is set to zero.

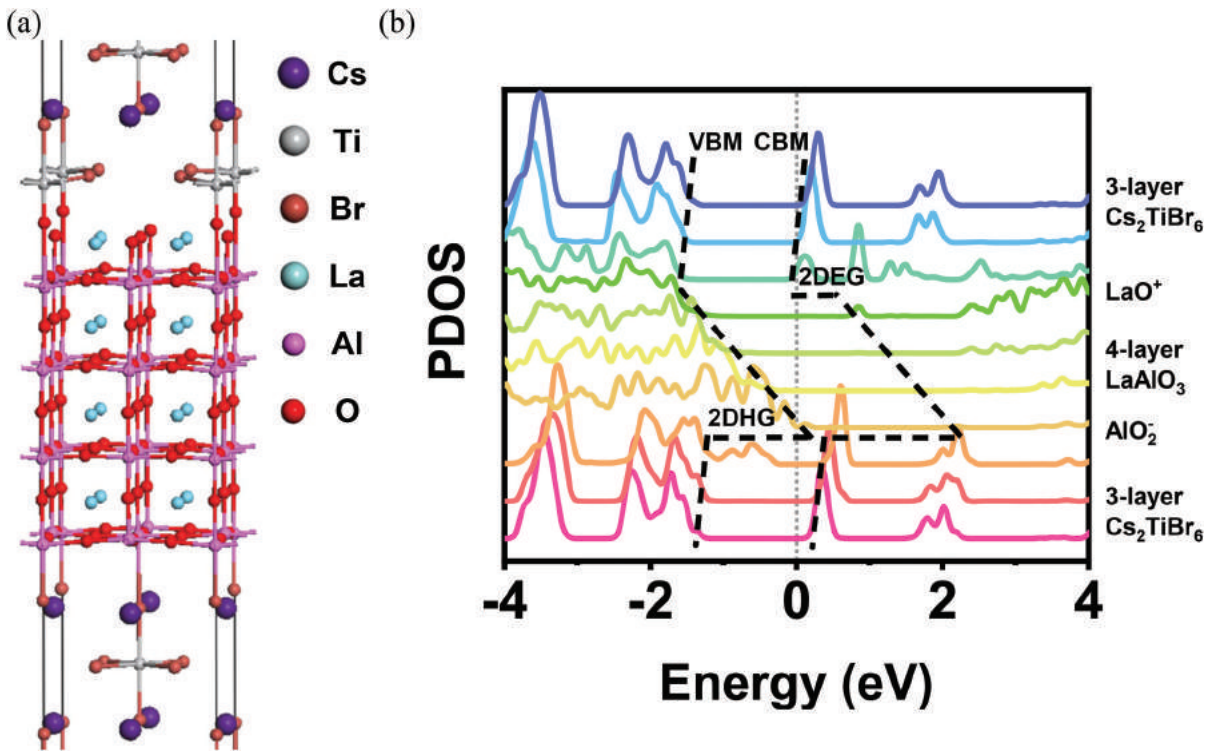

Fig. 7 (a) Atomic structure of asymmetrical Cs_2TiBr_6:$LaAlO_3$ interface model. Top interface is between LaO^+ and $TiBr_4$ layers and the bottom interface is between AlO_2^- and CsBr layers. (b) Layer-by-layer PDOSs in the interface model. The Fermi level is set to zero.

next superlattice period. It can also be seen that the top interface has straddling band line-up with obvious electron barrier from Cs_2TiBr_6 to $LaAlO_3$, whereas the bottom interface has staggered band line-up with hole barrier from $LaAlO_3$ to Cs_2TiBr_6 larger than 1.0 eV. The Fermi level is found to lie in higher energy than the CBM of Cs_2TiBr_6 at the top interface and in lower energy than the VBM of $LaAlO_3$ at the bottom interface. Consequently, with the band tilting, the top interface is n-type with 2D-confined electron gas and the bottom interface is p-type with 2D-confined hole gas. We also studied the influence of the quantum confinement effects by altering the numbers of layers of Cs_2TiBr_6 and $LaAlO_3$. It is found that the quantum confinement effects do not affect the existence of the two-dimensionally confined electron–hole gas, as shown in Fig. S7.† Although 2DEG has been widely observed, the coexistence of 2DEG and 2DHG at complementary interfaces in the same structure has only recently been evidenced.[37] On the other hand, in the $CsPbBr_3$:$LaAlO_3$ superlattice model with two asymmetric interfaces, it is noticed that the existence of 2DHG is largely not affected by the quantum confinement effects, while the existence of 2DEG is dependent on the layer thickness, as shown in Fig. S8.† In our test cases, 2DEG does not form until the number of $LaAlO_3$ layers is increased to eight. This provides the possibilities of tuning the 2DEG/2DHG systems by material selection and by precisely controlling the epitaxial growth thickness in the superlattice structures. Besides the most widely used $SrTiO_3$:$LaAlO_3$ superlattice, the PH (or dPH):$LaAlO_3$ superlattice may provide an alternative platform for the exciting physics of confined electron–hole systems and for developing applications. With the introduction of the non-oxygen anionic sublattice, new interfacial properties that have not been observed in the traditional all-PO interfaces are expected to emerge. Moreover, perovskite halides such as $CsPbBr_3$ and Cs_2TiBr_6 are optically active compared with $SrTiO_3$ and may open up new avenues for optically tunable perovskite electronics.

Conclusion

To conclude, various $CsPbBr_3$:ABO_3 and Cs_2TiBr_6:ABO_3 perovskite hetero-anionic-sublattice interfaces have been studied. Their functionalities in optoelectronics and nonconventional electronics have been assessed based on the interfacial band alignment properties. These POs are considered to be suitable CTMs for $CsPbBr_3$ and Cs_2TiBr_6 in either light-harvesting or light-emitting devices. Some typical binary TMOs have also been considered to be suitable CTMs for Cs_2TiBr_6-based PV applications. All-perovskite PH:PO and dPH:PO heterointerfaces are found to be defect- and dangling bond-free due to compatible crystal lattices, making POs potentially outperform conventional CTMs. In $CsPbBr_3$:$LaAlO_3$ and Cs_2TiBr_6:$LaAlO_3$ superlattice structures, a two-dimensionally confined electron–hole system is predicted at the two asymmetric interfaces. This finding, along with the optical activities of $CsPbBr_3$ and Cs_2TiBr_6, may spark developing applications of light–electron interaction in perovskite systems. This work presents new opportunities for perovskite heteroepitaxial interfaces.

Experimental section

First-principles calculations based on density functional theory (DFT) are carried out by using CASTEP.[38] The density functional of the generalized gradient approximation (GGA) type in the Perdew–Burke–Ernzerhof (PBE) flavor is used to present the electron–electron exchange correlation. Ultrasoft pseudopotentials with 380 eV cutoff energy for the plane wave basis set are used. $2 \times 2 \times 1$ *k*-point meshes are used for periodic supercell calculations of interfaces. The atomic positions are relaxed until the Hellmann–Feynman forces on the ions are smaller than 0.05 eV $Å^{-1}$ and the total energy convergence is within 2×10^{-6} eV.

Conflicts of interest

The authors declare no conflict of interest.

Acknowledgements

This work was partly supported by the National Natural Science Foundation (No. 61974082 and 61704096), Beijing Natural Science Foundation (No. 4164087), the Suzhou-Tsinghua Innovation Leading Program (No. 2016SZ0102), and the Brain-Science Special Program of Beijing (No. Z181100001518006). Computational resources were provided by the "Explorer 100" cluster system of Tsinghua National Laboratory for Information Science and Technology. D.C. is also grateful for support from the Tsinghua Spark Innovation Program and Tsinghua University Initiative Scientific Research Program.

References

1 A. K. Jena, A. Kulkarni and T. Miyasaka, *Chem. Rev.*, 2019, **119**, 3036.
2 L.-N. Quan, B. P. Rand, R. H. Friend, S. G. Mhaisalkar, T.-W. Lee and E. H. Sargent, *Chem. Rev.*, 2019, **119**, 7444.
3 L. Qiu, L. K. Ono and Y. Qi, *Mater. Today Energy*, 2018, **7**, 169.
4 Y. Zhou and Y. Zhao, *Energy Environ. Sci.*, 2019, **12**, 1495.
5 Z. Xiao, Z. Song and Y. Yan, *Adv. Mater.*, 2019, 1803792.
6 F. Igbari, Z.-K. Wang and L.-S. Liao, *Adv. Energy Mater.*, 2019, **9**, 1803150.
7 M.-G. Ju, M. Chen, Y. Zhou, H. F. Garces, J. Dai, L. Ma, N. P. Padture and X. C. Zeng, *ACS Energy Lett.*, 2018, **3**, 297.
8 M. Chen, M.-G. Ju, A. D. Carl, Y. Zong, R. L. Grimm, J. Gu, X. C. Zeng, Y. Zhou and N. P. Padture, *Joule*, 2018, **2**, 558.
9 D. Kong, D. Cheng, X. Wang, K. Zhang, H. Wang, K. Liu, H. Li, X. Sheng and L. Yin, *J. Mater. Chem. C*, 2020, **8**, 1591.

10 A. Fakharuddin, L. Schmidt-Mende, G. Garcia-Bemonte, R. Jose and I. Mora-Sero, *Adv. Energy Mater.*, 2017, **7**, 1700623.
11 Z. Zhou, S. Pang, Z. Liu, H. Xu and G. Cui, *J. Mater. Chem. A*, 2015, **3**, 19205.
12 A.-N. Cho and N.-G. Park, *ChemSusChem*, 2017, **10**, 3687.
13 A. Rajagopal, K. Yao and A. K. Y. Jen, *Adv. Mater.*, 2018, **30**, 1800455.
14 W.-J. Yin, J.-H. Yang, J. Kang, Y. Yan and S.-H. Wei, *J. Mater. Chem. A*, 2015, **3**, 8926.
15 R. Ramesh and D. G. Schlom, *Nat. Rev. Mater.*, 2019, **4**, 257.
16 P. Zubko, S. Gariglio, M. Gabay, P. Ghosez and J.-M. Triscone, *Annu. Rev. Condens. Matter Phys.*, 2011, **2**, 141.
17 J. Mannhart and D. G. Schlom, *Science*, 2010, **327**, 1607.
18 H. Y. Wang, Y. Iwasa, M. Kawasaki, B. Keimer, N. Nagaosa and Y. Tokura, *Nat. Mater.*, 2012, **11**, 103.
19 A. Bera, K. Wu, A. Sheikh, E. Alarousu, O. F. Mohammed and T. Wu, *J. Phys. Chem. C*, 2014, **118**, 28494.
20 S. S. Shin, E. J. Yeom, W. S. Yang, S. Hur, M. G. Kim, J. Im, J. Seo, J. H. Noh and S. I. Seok, *Science*, 2017, **356**, 167.
21 M. Neophytou, M. D. Bastiani, N. Gasparini, E. Aydin, E. Ugur, A. Seitkhan, F. Moruzzi, Y. Choaie, A. J. Ramadan, J. R. Troughton, R. Hallani, A. Savva, L. Tsetseris, S. Inal, D. Baran, F. Laquai, T. D. Anthopoulos, H. J. Snaith, S. D. Wolf and I. McCulloch, *ACS Appl. Energy Mater.*, 2019, **2**, 8090.
22 M. A. Haque, A. D. Sheikh, X. Guan and T. Wu, *Adv. Energy Mater.*, 2017, **7**, 1602803.
23 Z. Huang, D. Ouyang, C.-J. Shih, B. Yang and W. C. H. Choy, *Adv. Energy Mater.*, 2019, 1900903.
24 T. G. Liashenko, E. D. Cherotchenko, A. P. Pushkarev, V. Pakštas, A. Naujokaitis, S. A. Khubezhov, R. G. Polozkov, K. B. Agapev, A. A. Zakhidov, I. A. Shelykhae and S. V. Makarov, *Phys. Chem. Chem. Phys.*, 2019, **21**, 18930.
25 G. Cabello, L. Lillo, C. Caro, G. E. Buono-Core, B. Chornik, M. Flores, C. Carrasco and C. A. Rodriguez, *Ceram. Int.*, 2014, **40**, 7761.
26 N. Sata, M. Ishigame and S. Shin, *Solid State Ionics*, 1996, **86–88**, 629.
27 M. Noh, S. Choi, D. Lee, M. Cho, C. Jeon and Y. Lee, *New Phys.: Sae Mulli*, 2013, **63**, 939.
28 A. Klein, *Thin Solid Films*, 2012, **520**, 3721.
29 S. S. Shin, S. J. Lee and S. I. Seok, *Adv. Funct. Mater.*, 2019, 1900455.
30 M. A. Haque, A. D. Sheikh, X. Guan and T. Wu, *Adv. Energy Mater.*, 2017, **7**, 1602803.
31 G. Yang, H. Tao, P. Qin, W. Ke and G. Fang, *J. Mater. Chem. A*, 2016, **4**, 3970.
32 M. T. Greiner, M. G. Helander, W.-M. Tang, Z.-B. Wang, J. Qiu and Z.-H. Lu, *Nat. Mater.*, 2011, **11**, 76.
33 P. Qin, Q. He, D. Ouyang, G. Fang, W. C. H. Choy and G. Li, *Sci. China: Chem.*, 2017, **60**, 472.
34 J. Meyer, S. Hamwi, M. Kröger, W. Kowalsky, T. Riedl and A. Kahn, *Adv. Mater.*, 2012, **24**, 5408.
35 A. Ohtomo and H. Y. Hwang, *Nature*, 2004, **427**, 423.
36 N. Nakagawa, H. Y. Hwang and D. A. Muller, *Nat. Mater.*, 2006, **5**, 204.
37 H. Lee, N. Campbell, J. Lee, T. J. Asel, T. R. Paudel, H. Zhou, J. W. Lee, B. Noesges, J. Seo, B. Park, L. J. Brillson, S. H. Oh, E. Y. Tsymbal, M. S. Rzchowski and C. B. Eom, *Nat. Mater.*, 2018, **17**, 231.
38 S. J. Clark, M. D. Segall, C. J. Pickard, P. J. Hasnip, M. I. Probert, K. Refson and M. C. Payne, *Z. Kristallogr. – Cryst. Mater.*, 2005, **220**, 567.

